Contrib Mineral Petrol (2000) 138: 176–185

Wen-Sheng Horng · Paul C. Hess

Partition coefficients of Nb and Ta between rutile and anhydrous haplogranite melts

Received: 28 December 1998 / Accepted 27 September 1999

Abstract Partition coefficients (D) for Nb and Ta between rutile and haplogranite melts in the K_2O-Al_2O_3-SiO_2 system have been measured as functions of the K_2O/Al_2O_3 ratio, the concentrations of Nb_2O_5 and Ta_2O_5, the temperature, in air and at 1 atmosphere pressure. The Ds increase in value as the K* [$K_2O/(K_2O + Al_2O_3)$] molar ratio continuously decreases from highly peralkaline [K* $\sim$ 0.9] to highly peraluminous [K* $\sim$ 0.35] melts. The D values increase more dramatically with a unit decrease in K* in peraluminous melts than in peralkaline melts. This compositional dependence of Ds can be explained by the high activity of $NbAlO_4$ species in peraluminous melts and the high activity of KONb species (or low activity of $NbAlO_4$ species) in peralkaline melts. A coupled substitution, $Al^{+3} + Nb^{+5}$ (or Ta^{+5}) = $2Ti^{+4}$, accounts for the Ds of Nb (Ta) being much greater in peraluminous melts than in peralkaline melts because this substitution allows Nb (Ta) to enter into the rutile structure more easily. The Ds of Ta between rutile and melt are greater than those of Nb at comparable concentrations because the molecular electronic polarizability of Ta is weaker than that of Nb. The Nb^{+5} with a large polarizing power forms a stronger covalent bond with oxygen than Ta^{+5} with a small polarizing power. The formation of the strong bond, Nb-O, distorts the rutile structure more severely than the weak bond, Ta-O; therefore, it is easier for Ta to partition into rutile than for Nb. These results imply that the utilization of the Nb/Ta ratio in liquid as a petrogenetic indicator in granitic melts must be done with caution if rutile (or other TiO_2-rich phases) is a liquidus phase. The crystallization of rutile will increase the Nb/Ta ratio of the residual liquid because the Ds of Ta between rutile and melts are greater than those of Nb.

W.-S. Horng · P.C. Hess (✉)
Department of Geological Sciences,
Brown University, Providence, RI 02912, USA
Phone: (401)863-1925; Fax: (401)863-2058
E-mail: Wen-Sheng_Horng@brown.edu
E-mail: Paul_Hess@brown.edu

Editorial responsibility: T.L. Grove

Introduction

Nb-Ta-Ti-oxide minerals are important accessory phases in peraluminous and peralkaline granites and are common phases in rare element pegmatites (Cerny et al. 1999; Cerny 1992). These minerals are highly suited to study the detailed evolution of granitic systems, particularly the rare element pegmatites. These pegmatites typically are coarse grained, are heterogeneous on a variety of scales and commonly exhibit a well defined zonation in mineralogy and phase chemistry (Cerny 1992). Such pegmatites evolve under conditions of local rather than global equilibrium making it very difficult to trace the evolutionary path of the fractionated liquids (London 1992). The Ti-Nb-Ta oxide minerals with their variable compositions, varied paragenesis and ubiquity are useful index minerals and if their mineral-melt equilibria are fully calibrated can be used to monitor the complex liquid line of descent that characterizes individual pegmatite bodies. Nb-rutile, for example, shows strong compositional zoning and variation in Ta-Nb and variable resorption features which apparently reflect a complicated crystallization history (Abella et al. 1995). Rutile and columbite-tantalite are the most common and abundant Ti-Nb-Ta phases in pegmatites and a complete understanding of their paragenesis will provide important constraints on the petrogenesis of these bodies.

This paper is the second in a series of four which examines the solution properties of high field strength cations in anhydrous haplo-granite melts (papers I, II) and in wet analogues to peraluminous rhyolites (papers III, IV). The first paper investigates the interactions between M^{+5} cations, Ti^{+4} and alkali-aluminosilicate species by systematically measuring the liquidus of rutile

(Horng et al. 1999). In this paper, we measure the partition coefficients for Nb_2O_5 and Ta_2O_5 between rutile and peralkaline and peraluminous dry granite melts. In the last two papers, the solubility and phase chemistry of columbite-tantalite, Nb-Ta rutile, and cassiterite are determined by experiment, and the petrogenesis of these minerals in pegmatite melts is discussed (W.-S. Horng and P.C. Hess, in preparation). Our goals are to characterize the major cation interactions that control the phase equilibria and solution properties of such phases in highly evolved granitic melts.

Experimental method

Bulk compositions were made by mixing together appropriate amounts of reagent oxides and carbonate to yield glasses along the 80 mol% SiO_2 isopleth in the $SiO_2 + Al_2O_3 + K_2O$ system (Fig. 1). Glasses are either peralkaline [$K^* = K_2O/(K_2O + Al_2O_3)$ molar ratio > 0.5] with K^+ in molar excess of Al^{+3}, subaluminous ($K^* = 0.5$) with equal amounts of K^+ and Al^{+3}, or peraluminous ($K^* < 0.5$) with Al^{+3} in excess of K^+. An appropriate amount of TiO_2 is added to the base system in order to ensure rutile saturation. The concentration of added TiO_2 is approximately 1–2 mol% more than that obtained from Nb-free rutile saturation experiments with the same K* (Dickinson and Hess 1985). The Nb_2O_5 contents were varied from 0.28 to 7.89 mol%, whereas melts with 0.28 to 4.38 mol% Ta_2O_5 were studied. To understand the interaction between Nb and Ta in anhydrous haplogranite melts, three sets of experiments were conducted: Nb alone, Nb and Ta together, and Ta alone.

For each experiment, approximately 200–300 mg of the oxides and carbonate were packed into a porcelain combustion boat and decarbonated for four hours at approximately 950 °C and 1 atmosphere. The sample was then packed into a Pt capsule with one end welded and the other covered by a Pt lid. The charges were attached to a heavy gauge Pt wire and lowered into a vertical Del-Tech furnace at the desired temperature. The set of experiments using Nb alone were run at 1027, 1250, 1325 and 1400 °C, whereas the experiments (Nb and Ta together; Ta alone) were run at 1400 °C. The total run times were 32 hours, and the charges were quenched by dropping them into cold water (20 °C). In order to homogenize the sample and to overcome the kinetic barriers to nucleation, samples were reground once after eight hours of run time. Polished thin sections of random chips of the rutile-saturated charges were made, and the composition of the glass and the coexisting rutile were analyzed at Brown University with a Cameca Camebax (TM) electron microprobe, using a 15-kV accelerating potential, a 10-nA beam current, and a 25-μm beam diameter for glass and a focussed beam for rutile. Elements Si, Al, K, Ti, Nb, and Ta were counted for 10 s each on each point. Metal standards were used for Nb, Ta, Zr and Hf, whereas obsidian and basaltic glass were used for the major elements.

The same experiments were run for different durations (up to 48 hours) to test for equilibrium; it was observed that the length of the run time does not affect the saturation values and the partition coefficients of Nb and Ta. In addition, electron microprobe analyses of all charges reveal no compositional gradients for any component in the charge. Two reversal experiments have been conducted to check for equilibrium. In the first experiment (sample #: K*007a in Table 2), a glass saturated with rutile at 1325 °C was held at 1400 °C for 32 hours, including regrinding once after 8 hours of run time. In the second experiment (sample #: K*103a in Table 2), a glass saturated with rutile at 1400 °C was rerun at 1325 °C using the same experimental procedure. The Ds of Nb and Ta between rutile and melt and the concentration of other components in the two charges were nearly identical. These reversal experiments confirm that Nb-Ta exchange equilibrium was achieved in these experiments.

Results

Melts doped with Nb_2O_5

Figure 2 gives the partition coefficients (Ds) of Nb between rutile and melt in experiments doped with 0.28, 1.36, 4.38, and 7.89 mol% Nb_2O_5 at 1400 °C as a function of K*. Table 1 gives the compositions of the glasses and the coexisting rutile. The Ds of Nb decrease with increasing K*, and they decrease more dramatically in peraluminous compositions than in peralkaline compositions. Table 2 gives the compositions of the glasses and the coexisting rutile in experiments doped with 1.36 mol% Nb_2O_5 at 1027, 1250, 1325, and 1400 °C, and Fig. 3 illustrates the dependence of the Ds of Nb on

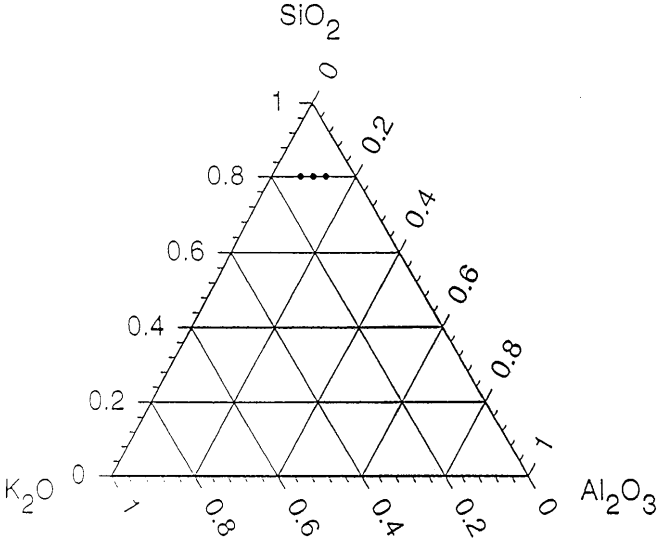

Fig. 1 Ternary base mixtures lie along the 80 mol% SiO_2 isopleth. The melts are peraluminous, subaluminous, and peralkaline

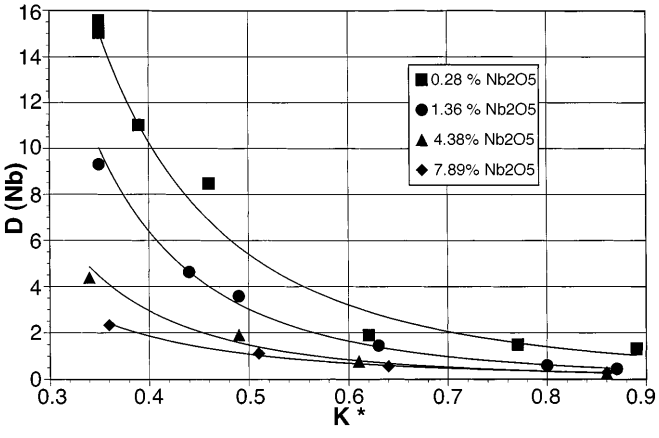

Fig. 2 Dependence of Ds of Nb between rutile and melt on K* for different amounts of Nb_2O_5 at $T = 1400$ °C and $P = 1$ atmosphere

Table 1 Experimental conditions and chemical composition of rutile and coexisting haplogranite melts doped with Nb_2O_5 at 1400 °C (mol%)

Sample	Doped Nb_2O_5 (mol%)	Phase	SiO_2	K_2O	Al_2O_3	TiO_2	Nb_2O_5	K*	D_{Nb}
K*001	0.28	Melt	76.12 ± 0.57[a]	5.97 ± 0.12	11.05 ± 0.21	6.66 ± 0.17	0.21 ± 0.03	0.35	15.57
		Rutile	0.24 ± 0.04	0.17 ± 0.03	3.19 ± 0.11	93.13 ± 0.72	3.27 ± 0.12		
K*001[b]	0.28	Melt	76.07 ± 0.67	5.86 ± 0.14	11.07 ± 0.25	6.78 ± 0.19	0.22 ± 0.05	0.35	15.05
		Rutile	0.25 ± 0.05	0.11 ± 0.03	3.15 ± 0.15	93.18 ± 0.69	3.31 ± 0.14		
K*002	0.28	Melt	75.10 ± 0.71	6.57 ± 0.09	10.17 ± 0.19	7.91 ± 0.15	0.25 ± 0.04	0.39	11.01
		Rutile	0.24 ± 0.06	0.26 ± 0.04	2.88 ± 0.12	93.86 ± 0.73	2.75 ± 0.18		
K*003	0.28	Melt	72.23 ± 0.58	9.64 ± 0.13	11.48 ± 0.21	8.36 ± 0.23	0.28 ± 0.06	0.46	8.48
		Rutile	0.52 ± 0.10	0.31 ± 0.08	2.78 ± 0.15	94.00 ± 0.64	0.67 ± 0.09		
K*004	0.28	Melt	66.57 ± 0.71	9.67 ± 0.21	5.97 ± 0.10	17.42 ± 0.15	0.36 ± 0.05	0.62	1.89
		Rutile	0.06 ± 0.02	0.11 ± 0.03	0.41 ± 0.08	98.74 ± 0.87	0.67 ± 0.08		
K*005	0.28	Melt	59.89 ± 0.72	10.39 ± 0.27	3.03 ± 0.31	26.48 ± 0.41	0.21 ± 0.05	0.77	1.49
		Rutile	0.06 ± 0.03	0.22 ± 0.05	0.15 ± 0.04	99.26 ± 0.79	0.31 ± 0.05		
K*006	0.28	Melt	55.93 ± 0.63	10.71 ± 0.18	1.37 ± 0.13	31.78 ± 0.37	0.22 ± 0.04	0.89	1.31
		Rutile	0.07 ± 0.04	0.10 ± 0.03	0.05 ± 0.02	99.55 ± 0.68	0.28 ± 0.03		
K*007	1.36	Melt	77.37 ± 0.67	5.68 ± 0.19	10.30 ± 0.25	5.75 ± 0.19	0.91 ± 0.11	0.35	9.31
		Rutile	0.29 ± 0.05	0.10 ± 0.03	8.19 ± 0.34	82.95 ± 0.79	8.48 ± 0.23		
K*008	1.36	Melt	74.81 ± 0.75	7.38 ± 0.21	9.30 ± 0.17	7.45 ± 0.17	1.06 ± 0.17	0.44	4.63
		Rutile	0.41 ± 0.07	0.26 ± 0.05	4.83 ± 0.23	89.61 ± 0.68	4.89 ± 0.18		
K*009	1.36	Melt	75.79 ± 0.81	7.60 ± 0.27	7.88 ± 0.19	7.60 ± 0.13	1.13 ± 0.15	0.49	3.58
		Rutile	0.37 ± 0.04	0.20 ± 0.05	4.34 ± 0.17	91.07 ± 0.72	4.02 ± 0.24		
K*010	1.36	Melt	66.68 ± 0.59	9.10 ± 0.15	5.42 ± 0.14	17.62 ± 0.21	1.18 ± 0.19	0.63	1.45
		Rutile	0.12 ± 0.03	0.23 ± 0.05	0.79 ± 0.08	97.15 ± 0.64	1.71 ± 0.19		
K*011	1.36	Melt	58.10 ± 0.71	10.16 ± 0.21	2.54 ± 0.17	27.86 ± 0.15	1.34 ± 0.14	0.80	0.60
		Rutile	0.12 ± 0.04	0.11 ± 0.03	0.20 ± 0.05	98.76 ± 0.62	0.81 ± 0.08		
K*012	1.36	Melt	55.89 ± 0.67	10.86 ± 0.31	1.64 ± 0.09	30.56 ± 0.25	1.32 ± 0.21	0.87	0.45
		Rutile	0.05 ± 0.03	0.12 ± 0.04	0.10 ± 0.05	99.17 ± 0.83	0.59 ± 0.06		
K*013	4.38	Melt	75.87 ± 0.73	5.34 ± 0.13	10.35 ± 0.21	5.07 ± 0.21	3.37 ± 0.13	0.34	4.39
		Rutile	0.22 ± 0.04	0.08 ± 0.02	15.43 ± 0.29	69.49 ± 0.68	14.78 ± 0.31		
K*014	4.38	Melt	73.00 ± 0.69	7.42 ± 0.17	7.82 ± 0.19	8.59 ± 0.15	3.87 ± 0.17	0.49	1.90
		Rutile	0.12 ± 0.03	0.13 ± 0.04	6.25 ± 0.16	86.16 ± 0.79	7.35 ± 0.28		
K*015	4.38	Melt	66.75 ± 0.57	8.57 ± 0.15	5.39 ± 0.13	14.73 ± 0.31	4.55 ± 0.19	0.61	0.77
		Rutile	0.37 ± 0.04	0.10 ± 0.03	2.55 ± 0.15	93.49 ± 0.63	3.49 ± 0.21		
K*016	4.38	Melt	55.87 ± 0.59	10.12 ± 0.29	1.71 ± 0.11	27.34 ± 0.34	4.96 ± 0.16	0.86	0.26
		Rutile	0.07 ± 0.02	0.09 ± 0.03	0.54 ± 0.10	98.08 ± 0.78	1.29 ± 0.11		
K*017	7.80	Melt	72.37 ± 0.68	5.15 ± 0.19	9.36 ± 0.31	6.04 ± 0.17	7.08 ± 0.23	0.36	2.33
		Rutile	0.06 ± 0.02	0.04 ± 0.02	16.34 ± 0.34	67.11 ± 0.77	16.51 ± 0.31		
K*018	7.80	Melt	68.32 ± 0.58	6.96 ± 0.21	6.58 ± 0.19	10.44 ± 0.19	7.70 ± 0.18	0.51	1.11
		Rutile	0.09 ± 0.02	0.10 ± 0.03	7.38 ± 0.25	83.88 ± 0.68	8.56 ± 0.32		
K*019	7.80	Melt	62.16 ± 0.63	8.30 ± 0.19	4.59 ± 0.21	16.99 ± 0.27	7.95 ± 0.17	0.64	0.56
		Rutile	0.04 ± 0.02	0.07 ± 0.03	3.18 ± 0.21	92.27 ± 0.69	4.43 ± 0.29		
K*020	7.80	Melt	58.25 ± 0.71	8.31 ± 0.31	1.41 ± 0.12	22.88 ± 0.25	9.15 ± 0.21	0.86	0.29
		Rutile	0.03 ± 0.02	0.04 ± 0.02	0.90 ± 0.08	96.42 ± 0.83	2.61 ± 0.17		

[a] The values before the ± symbol refer to analytic results (mol%), and the values after the ± symbol denote one standard deviation (wt%)
[b] Long duration: 48 hours, all others were run for 32 hours

temperature. For a given K*, the Ds of Nb decrease systematically with decreasing run temperature.

Melts doped with Ta_2O_5

Figure 4 displays the Ds of Ta between rutile and melt as a function of K* for experiments doped with 0.28 and 4.38 mol% Ta_2O_5 at 1400 °C. Table 3 lists the compositions of the glasses and the coexisting rutile. The Ds of Ta decrease as the amount of Ta_2O_5 in the starting composition increases. The Ds of Ta show a compositional dependence similar to the equivalent experiments doped with only Nb_2O_5 at 1400 °C. For a given K*, Ds of Ta are approximately twice as large as those of Nb in equivalent Nb experiments (Fig. 4).

Melts doped with Nb_2O_5 and Ta_2O_5 together

Figure 5 displays the Ds of Nb and Ta between rutile and melts as a function of K* for experiments doped with 0.28 mol% Nb_2O_5 and 0.28 mol% Ta_2O_5 at 1400 °C, and Table 4 lists the compositions of the glasses and the coexisting rutile. The D versus K* trends in Fig. 4 reveal that the Ds of Ta and Nb exhibit similar patterns of compositional dependence. The Ds of Ta are approximately twice as large as those of Nb for a given K*.

Table 2 Experimental conditions and chemical composition of rutile and coexisting haplogranite melts doped with 1.36 mol% Nb_2O_5 (mol%)

Sample	T (°C)	Phase	SiO_2	K_2O	Al_2O_3	TiO_2	Nb_2O_5	K*	D_{Nb}
K*007	1400	Melt	77.37 ± 0.67[a]	5.68 ± 0.19	10.30 ± 0.25	5.75 ± 0.19	0.91 ± 0.11	0.35	9.31
		Rutile	0.29 ± 0.05	0.10 ± 0.03	8.19 ± 0.34	82.95 ± 0.79	8.48 ± 0.23		
K*007a[b]	1400	Melt	77.73 ± 0.73	5.39 ± 0.23	10.36 ± 0.31	5.64 ± 0.24	0.88 ± 0.08	0.34	9.36
		Rutile	0.51 ± 0.06	0.15 ± 0.03	8.30 ± 0.36	82.79 ± 0.71	8.24 ± 0.27		
K*008	1400	Melt	74.81 ± 0.75	7.38 ± 0.21	9.30 ± 0.17	7.45 ± 0.17	1.06 ± 0.17	0.44	4.63
		Rutile	0.41 ± 0.07	0.26 ± 0.05	4.83 ± 0.23	89.61 ± 0.68	4.89 ± 0.18		
K*009	1400	Melt	75.79 ± 0.81	7.60 ± 0.27	7.88 ± 0.19	7.60 ± 0.13	1.13 ± 0.15	0.49	3.58
		Rutile	0.37 ± 0.04	0.20 ± 0.05	4.34 ± 0.17	91.07 ± 0.72	4.02 ± 0.24		
K*010	1400	Melt	66.68 ± 0.59	9.10 ± 0.15	5.42 ± 0.14	17.62 ± 0.21	1.18 ± 0.19	0.63	1.45
		Rutile	0.12 ± 0.03	0.23 ± 0.05	0.79 ± 0.08	97.15 ± 0.64	1.71 ± 0.19		
K*011	1400	Melt	58.10 ± 0.71	10.16 ± 0.21	2.54 ± 0.17	27.86 ± 0.15	1.34 ± 0.14	0.80	0.60
		Rutile	0.12 ± 0.04	0.11 ± 0.03	0.20 ± 0.05	98.76 ± 0.62	0.81 ± 0.08		
K*012	1400	Melt	55.89 ± 0.67	10.86 ± 0.31	1.64 ± 0.09	30.56 ± 0.25	1.32 ± 0.21	0.87	0.45
		Rutile	0.05 ± 0.03	0.12 ± 0.04	0.10 ± 0.05	99.17 ± 0.83	0.59 ± 0.06		
K*101	1325	Melt	79.02 ± 0.81	5.03 ± 0.17	8.66 ± 0.21	5.99 ± 0.19	1.30 ± 0.15	0.37	3.30
		Rutile	0.26 ± 0.04	0.49 ± 0.05	4.23 ± 0.19	90.69 ± 0.87	4.34 ± 0.21		
K*102	1325	Melt	76.70 ± 0.75	7.45 ± 0.21	7.15 ± 0.19	7.40 ± 0.23	1.30 ± 0.19	0.51	2.1
		Rutile	0.44 ± 0.06	0.73 ± 0.07	2.64 ± 0.16	93.42 ± 0.79	2.76 ± 0.15		
K*103	1325	Melt	62.96 ± 0.68	10.73 ± 0.25	3.08 ± 0.17	21.83 ± 0.37	1.40 ± 0.11	0.78	0.55
		Rutile	0.08 ± 0.02	0.24 ± 0.04	0.23 ± 0.05	98.68 ± 0.74	0.76 ± 0.08		
K*103a[c]	1325	Melt	63.76 ± 0.73	10.18 ± 0.19	3.17 ± 0.23	21.54 ± 0.17	1.35 ± 0.17	0.76	0.50
		Rutile	0.20 ± 0.04	0.26 ± 0.05	0.34 ± 0.06	98.53 ± 0.91	0.67 ± 0.07		
K*104	1325	Melt	57.20 ± 0.65	11.39 ± 0.18	1.35 ± 0.14	28.56 ± 0.38	1.50 ± 0.12	0.89	0.4
		Rutile	0.08 ± 0.03	0.15 ± 0.04	0.17 ± 0.03	99.00 ± 0.83	0.60 ± 0.09		
K*105	1250	Melt	76.21 ± 0.74	5.13 ± 0.16	8.74 ± 0.28	8.6 ± 0.18	1.32 ± 0.16	0.37	–
		Cristobalite	99.99 ± 0.78	–	–	–	–		
K*106	1250	Melt	77.40 ± 0.68	7.83 ± 0.22	7.46 ± 0.21	6.32 ± 0.21	1.31 ± 0.17	0.51	1.52
		Rutile	0.14 ± 0.03	0.35 ± 0.07	1.55 ± 0.10	95.98 ± 0.78	1.99 ± 0.21		
K*107	1250	Melt	71.19 ± 0.64	9.06 ± 0.18	5.49 ± 0.18	12.47 ± 0.26	1.80 ± 0.15	0.62	0.65
		Rutile	0.04 ± 0.02	0.15 ± 0.03	0.78 ± 0.08	97.86 ± 0.83	1.17 ± 0.09		
K*108	1250	Melt	58.41 ± 0.61	11.91 ± 0.24	1.52 ± 0.12	26.66 ± 0.24	1.50 ± 0.12	0.89	0.23
		Rutile	0.07 ± 0.03	0.27 ± 0.05	0.16 ± 0.03	99.16 ± 0.78	0.35 ± 0.08		
K*109	1027	Melt	75.96 ± 0.66	5.42 ± 0.19	8.57 ± 0.23	8.70 ± 0.15	1.35 ± 0.21	0.39	–
		Cristobalite	99.99 ± 0.88	–	–	–	–		
K*110	1027	Melt	76.04 ± 0.68	8.93 ± 0.23	4.15 ± 0.17	9.42 ± 0.21	1.48 ± 0.18	0.68	0.5
		Rutile	0.77 ± 0.05	0.34 ± 0.4	0.17 ± 0.03	97.98 ± 0.84	0.74 ± 0.07		
K*111	1027	Melt	69.86 ± 0.72	11.64 ± 0.17	3.86 ± 0.18	13.14 ± 0.19	1.50 ± 0.13	0.75	0.28
		Rutile	0.34 ± 0.03	0.42 ± 0.08	0.17 ± 0.04	98.65 ± 0.79	0.42 ± 0.05		
K*112	1027	Melt	65.53 ± 0.67	12.17 ± 0.15	1.84 ± 0.13	18.68 ± 0.25	1.77 ± 0.15	0.87	0.19
		Rutile	0.33 ± 0.05	0.66 ± 0.10	0.17 ± 0.02	98.51 ± 0.83	0.33 ± 0.04		
NbA01[d]	1350	Melt	76.57 ± 0.71	4.71 ± 0.21	12.19 ± 0.23	0	6.52 ± 0.25	0.28	7.72
		$NbAlO_4$	0.53 ± 0.07	0.07 ± 0.03	49.05 ± 0.31	0	50.34 ± 0.45		

[a] The values before the ± symbol refer to analytic results (mol%), and the values after the ± symbol denote one standard deviation (wt%)

[b] Reversal experiment (sample #: K*007a) for rerunning charge quenched at 1325 °C at 1400 °C, see text

[c] Reversal experiment (sample #: K*103a) for rerunning charge quenched at 1400 °C at 1325 °C, see text

[d] Saturation experiment for the crystalline phase niobium aluminate ($NbAlO_4$) in peraluminous melts at P = 1 atmosphere, see text

Discussion

Melts doped with Nb_2O_5

The coupled substitution ($Al^{+3} + Nb^{+5} = 2Ti^{+4}$)

In the Nb_2O_5-doped experiments, the composition of rutile coexisting with peralkaline melts is almost pure TiO_2, whereas the composition of rutile (Nb-rutile) coexisting with peraluminous melts shows substantial solid solution of Nb_2O_5 and Al_2O_3 (Table 1). The molar ratio of Al_2O_3/Nb_2O_5 in the Nb-rutile approximates one, and the contents of Al_2O_3 and Nb_2O_5 increase as K* decreases (Fig. 6). This suggests that the coupled substitution, $Al^{+3} + Nb^{+5} = 2Ti^{+4}$, controls the solubility of Nb in rutile in peraluminous melts. This mechanism for coupled substitution was also argued for by McCallum and Charette (1978) based on the experiments of Nb partitioning between rutile and basaltic liquid.

The Nb-Al-rutile in peraluminous melts is a good analog to naturally occurring Nb-rutile (or ilmenorutile) in granite pegmatites except that Fe^{+3} typically replaces Al^{+3} as the charge balancing species for Nb^{+5}. The ilmenorutile [$(Ti, Nb, Fe^{+3})_3O_6$] has the same structure as rutile, an expected consequence of the similarity of ionic radii of Al^{+3} (0.53Å) and Fe^{+3} (0.55Å) for sixfold coordination with oxygen (Foord 1982).

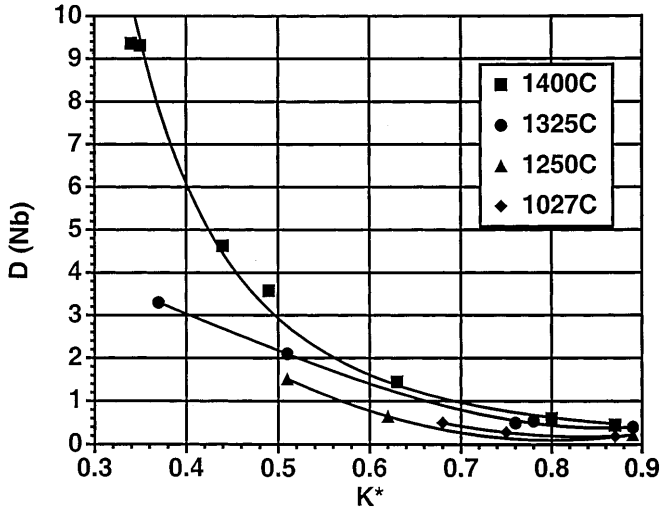

Fig. 3 Dependence of Ds of Nb between rutile and melt on temperature in experiments doped with 1.36 mol% Nb_2O_5 at $P = 1$ atmosphere

Partition coefficients (Ds) of Nb

In the experiments doped with Nb_2O_5 at 1400 °C, the Ds of Nb between rutile and melts decrease with increasing K* (Fig. 2). The relatively high Nb_2O_5 contents of rutile in peraluminous melts no doubt reflect the high activities of $NbAlO_4$ melt species. The Nb^{+5} needs Al^{+3} to be charge balanced in the form of a coupled substitution, $Nb^{+5} + Al^{+3} = 2Ti^{+4}$, when Nb^{+5} partitions into the rutile structure. In peraluminous melts, Al in excess of K exists as triclusters (AlOAl) without SiO_4 tetrahedra [or possibly triclusters (AlOSi) with SiO_4 tetrahedra], and all K is incorporated in $KO^{[4]}Al$ complexes ($KO^{[4]}Al$ where [4] refers to the number of bridging oxygens in AlO_4 tetrahedra) as a charge balancing cation (Lacey 1968; Mysen et al. 1980, 1981; McMillan and Piriou 1982; Sato et al. 1991; Gan and Hess 1992). The AlOAl bonds (or AlOSi) are less stable than KOAl bonds because only the latter species are locally charge balanced.

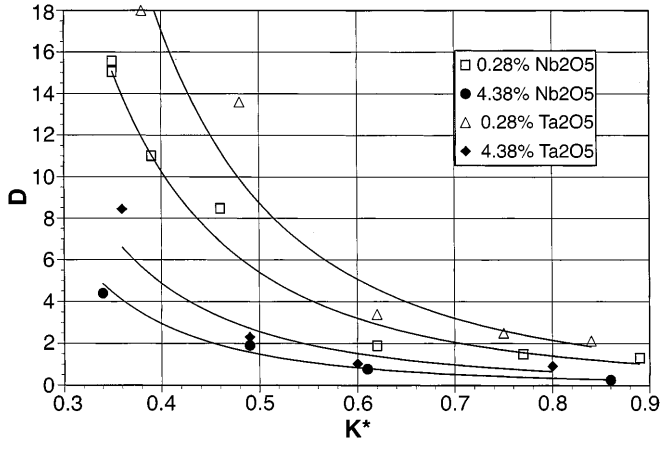

Fig. 4 Dependence of Ds of Ta and Nb between rutile and melt on K*

In contrast, the oxygens shared by the Al-tricluster are either overbonded or underbonded depending on the coordination of Al (Sharma et al. 1978; Virgo et al. 1979; Mysen et al. 1980, 1981, 1982; McMillan et al. 1982; Sato et al. 1991; Gan and Hess 1992). The relatively less stable AlOAl species in peraluminous melts react with Nb_2O_5 to form a locally charge balanced species according to the homogeneous equilibria

$$AlOAl_{(melt)} + NbONb_{(melt)} = 2NbOAl_{(melt)} \quad . \tag{1}$$

The validity of Eq. (1) as a solution mechanism is supported by a number of observations. First, the fact that $NbAlO_4$ enters into solid solution with the rutile structure is evidence that such species are intrinsically stable. Experience has indicated that the stability of melt species is typically indicated by the stability of the corresponding crystalline species (e.g., Hess 1995). Indeed, if this concept is taken to the extreme, we might expect that the $NbOAl_{(melt)}$ species would preferentially be located within locally TiO_2 rich regions of the peraluminous melts. Secondly, we found by experiment that the crystalline phase, niobium aluminate $NbAlO_4$, is a liquidus phase in the TiO_2-free peraluminous melts at 1350 °C (Table 2). The saturated melt contains 6.5 mol% Nb_2O_5 and the ratio of Nb_2O_5 to excess Al_2O_3 is only slightly less than unity [$Nb_2O_5/Al_2O_{3(excess)} = 0.87$], giving a strong indication that the most important Nb species in the melt is, indeed, $NbAlO_4$.

Finally, Gan and Hess (1992) used NMR and Raman spectroscopy to show that $AlPO_4$ species were stable in peraluminous melts and the solution mechanisms were:

$$2AlOSi + POP = 2AlOP + SiOSi$$

or

$$2AlOAl + POP = 2AlOP \tag{2}$$

in direct correspondence to the homogeneous equilibria indicated for $AlNbO_4$. Horng et al. (1999) found by experiment that the variation of rutile solubility in melts of peraluminous composition doped with varying amounts of P_2O_5 or Nb_2O_5 behaved similarly. The solubility mechanism of these M^{+5} cations, therefore, appears to be similar if not identical.

The rutile-melt Nb partition coefficients in peralkaline melts are much smaller than those in peraluminous melts. Whereas the composition of rutile in peraluminous melts has a Nb/Al $\sim$ 1 (in moles), rutile in the most peralkaline melts has Nb/Al > 1. Rutile in peralkaline melts with K* > 0.80, for example, has Nb/Al = 2–4 (Table 1). These observations emphasize two points regarding the solution mechanism in peralkaline melts. First, the activity of $NbAlO_4$ in peralkaline melts is low. Secondly, because the preferred solution mechanism of Nb in rutile requires a coupled substitution with Al, the $AlNbO_4$ species does not account for Nb/Al = 2–4 in rutile. This suggests that an additional solution mechanism of Nb is possible in rutile. A likely solution mechanism in rutile is

$$4Nb^{+5} + Vac = 5Ti^{+4} \tag{3}$$

Table 3 Experimental conditions and chemical composition of saturated rutile and coexisting haplogranite melts doped with different amounts of Ta_2O_5 at 1400 °C (mol%)

Sample	Doped Ta_2O_5 (mol%)	Phase	SiO_2	K_2O	Al_2O_3	TiO_2	Ta_2O_5	K*	D_{Ta}
K*301	0.28	Melt	76.73 ± 0.71[a]	6.43 ± 0.17	10.36 ± 0.22	6.43 ± 0.15	0.17 ± 0.05	0.38	18.00
		Rutile	0.52 ± 0.05	0.19 ± 0.03	2.25 ± 0.17	94.06 ± 0.86	2.98 ± 0.21		
K*302	0.28	Melt	76.71 ± 0.68	7.46 ± 0.15	8.13 ± 0.18	7.54 ± 0.14	0.17 ± 0.04	0.48	13.60
		Rutile	0.19 ± 0.04	0.47 ± 0.05	2.38 ± 0.25	94.58 ± 0.79	2.37 ± 0.32		
K*303	0.28	Melt	66.98 ± 0.59	9.19 ± 0.23	5.72 ± 0.15	17.90 ± 0.24	0.21 ± 0.03	0.62	3.39
		Rutile	0.20 ± 0.03	0.34 ± 0.05	0.51 ± 0.04	98.25 ± 0.81	0.69 ± 0.07		
K*304	0.28	Melt	62.95 ± 0.69	9.51 ± 0.18	3.20 ± 0.14	24.11 ± 0.22	0.23 ± 0.05	0.75	2.49
		Rutile	0.08 ± 0.02	0.19 ± 0.03	0.26 ± 0.05	98.91 ± 0.88	0.57 ± 0.06		
K*305	0.28	Melt	60.27 ± 0.56	10.25 ± 0.28	1.96 ± 0.19	27.28 ± 0.24	0.24 ± 0.04	0.84	2.12
		Rutile	0.04 ± 0.02	0.09 ± 0.02	0.15 ± 0.03	99.22 ± 0.83	0.51 ± 0.06		
K*311	4.38	Melt	81.72 ± 0.74	4.52 ± 0.15	8.13 ± 0.21	2.48 ± 0.12	3.15 ± 0.13	0.36	8.44
		Rutile	0.63 ± 0.07	0.24 ± 0.04	26.85 ± 0.32	44.71 ± 0.74	26.57 ± 0.31		
K*312	4.38	Melt	72.80 ± 0.68	6.86 ± 0.19	7.09 ± 0.12	8.72 ± 0.21	4.54 ± 0.21	0.49	2.30
		Rutile	0.75 ± 0.10	0.16 ± 0.03	9.35 ± 0.19	79.29 ± 0.93	10.44 ± 0.16		
K*313	4.38	Melt	72.09 ± 0.62	7.02 ± 0.22	4.50 ± 0.19	11.96 ± 0.25	4.24 ± 0.17	0.60	1.02
		Rutile	0.68 ± 0.07	0.07 ± 0.02	4.41 ± 0.15	90.50 ± 0.86	4.34 ± 0.26		
K*314	4.38	Melt	54.82 ± 0.65	15.30 ± 0.15	3.73 ± 0.14	21.08 ± 0.29	5.07 ± 0.16	0.80	0.91
		Rutile	0.88 ± 0.07	0.18 ± 0.03	4.56 ± 0.16	89.76 ± 0.72	4.62 ± 0.19		

[a] The values before the ± symbol refer to analytic results (mol%), and the values after the ± symbol denote one standard deviation (wt%)

where Vac represents the vacancy created by the substitution.

The low activities of $AlNbO_4$ in these peralkaline melts imply low activities of excess Al species. Indeed, according to the homogeneous equilibria

$$AlOAl + NbONb = 2NbOAl$$

or

$$2AlOSi + NbONb = 2NbOAl + SiOSi \quad , \tag{4}$$

low activities of AlOAl or AlOSi require low activities of the corresponding NbOAl species. In the simplest model of peralkaline melts, the Al species are all incorporated in the relatively stable $KAlO_2$ species (Dickinson and Hess 1985; Hess 1991), leaving little Al in excess. In this case, the solution mechanism for Nb_2O_5 is

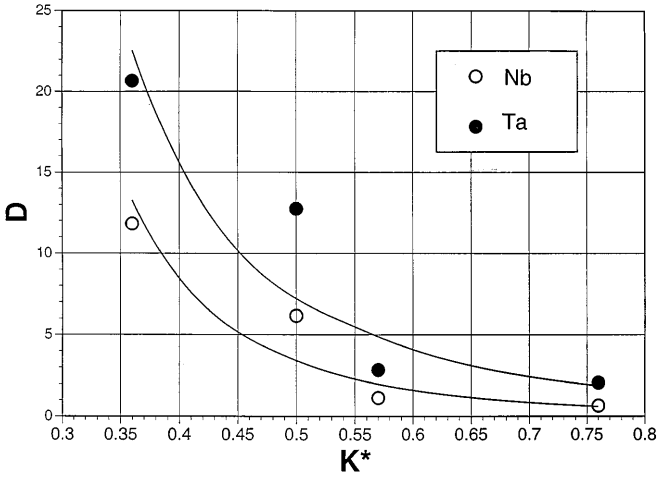

Fig. 5 Dependence of Ds of Nb and Ta between rutile and melt on K* for experiments doped with 0.28 mol% Nb_2O_5 and 0.28 mol% Ta_2O_5 at 1 atmosphere

$$2KOSi + NbONb = 2KONb + SiOSi \tag{5}$$

where niobate species are stabilized by excess alkalis (Hess 1995). This model is not totally accurate, however. Note that the $AlNbO_4$ content of rutile is not negligible and increases to about one mole percent even in the most peralkaline melts at high Nb_2O_5 contents (Table 1). From what was argued earlier, a finite $NbAlO_4$ concentration in rutile requires a finite activity of $NbAlO_4$ in the peralkaline melts. A small fraction of Nb_2O_5 is probably involved in the homogeneous equilibrium

$$KOAl + NbONb = AlONb + KONb \tag{6}$$

wherein the Nb reacts with tetrahedral aluminum charge balanced by potassium. Such a solution mechanism apparently exists in P_2O_5-bearing subaluminous melts and perhaps also in peralkaline melts (Gan et al. 1994; Gan and Hess 1992; Horng et al. 1999).

The content of $NbAlO_4$ species in peralkaline melts must be very small, however. A reasonable estimate of the $NbAlO_4$ concentration is obtained by applying the bulk partition coefficient obtained for Nb in peraluminous melts to the species distribution of $NbAlO_4$ in rutile and peralkaline melts. It follows that the $NbAlO_4$ content in peralkaline melts is roughly an order of magnitude smaller than the $NbAlO_4$ content of coexisting rutile.

The substitution of Nb^{+5} and Al^{+3} for $2Ti^{+4}$ probably distorts the rutile structure, since the charges and the ionic radii of Nb^{+5} and Al^{+3} (Nb^{+5} = 0.64 Å; Al^{+3} = 0.53 Å for six-fold coordination with oxygen) differ slightly from those of Ti^{+4} (r = 0.605 Å for the same coordination number) (Shannon and Prewitt 1969). Therefore, the accommodation of Nb_2O_5 in rutile increases more slowly than the amount of Nb_2O_5 added

Table 4 Experimental conditions and chemical composition of rutile and coexisting haplogranite melts doped with 0.28 mol% Nb_2O_5 and 0.28 mol% Ta_2O_5 together at 1 atmosphere

Sample	T (°C)	Phase	SiO_2	K_2O	Al_2O_3	TiO_2	Nb_2O_5	Ta_2O_5	K*	D_{Nb}	D_{Ta}
K*201	1400	Melt	79.78 ± 0.79[a]	5.86 ± 0.19	9.91 ± 0.24	6.19 ± 0.17	0.30 ± 0.05	0.24 ± 0.03	0.36	11.82	20.67
		Rutile	0.07 ± 0.02	0.17 ± 0.04	8.85 ± 0.21	82.48 ± 0.86	3.54 ± 0.22	4.88 ± 0.17			
K*202	1400	Melt	74.60 ± 0.81	8.34 ± 0.23	8.43 ± 0.31	8.17 ± 0.21	0.25 ± 0.03	0.22 ± 0.04	0.50	6.16	12.75
		Rutile	0.45 ± 0.05	0.12 ± 0.02	6.09 ± 0.19	89.59 ± 0.74	1.56 ± 0.12	2.77 ± 0.15			
K*203	1400	Melt	73.08 ± 0.68	7.80 ± 0.29	5.88 ± 0.23	12.71 ± 0.32	0.30 ± 0.04	0.23 ± 0.03	0.57	1.14	2.85
		Rutile	0.53 ± 0.04	0.24 ± 0.04	0.62 ± 0.06	97.62 ± 0.82	0.35 ± 0.05	0.64 ± 0.05			
K*204	1400	Melt	60.95 ± 0.71	11.09 ± 0.16	3.47 ± 0.18	23.96 ± 0.42	0.31 ± 0.03	0.23 ± 0.04	0.76	0.66	2.07
		Rutile	0.08 ± 0.02	0.09 ± 0.03	0.28 ± 0.05	98.87 ± 0.79	0.20 ± 0.04	0.48 ± 0.03			

[a] The values before ± symbol refer to analytic results (mol%), and the values after the ± symbol denote one standard deviation (wt%)

to the starting composition, and perhaps approaches a maximum limit. The melt structure is more flexible and thus more able to accommodate increasing amounts of Nb_2O_5. In the peraluminous melts, the Ds of Nb, therefore, decrease systematically and the slope of the D versus K* curves becomes shallower as the amount of Nb_2O_5 added to the starting composition increases. In contrast, because little Nb_2O_5 partitions into rutile in peralkaline melts, the Ds of Nb decrease more slowly as the amount of Nb_2O_5 in the starting composition increases.

Melts doped with Ta_2O_5

The D versus K* curves for Ta in Fig. 4 are similar to those found in equivalent experiments doped with the same amount of Nb_2O_5. This suggests that the partitioning of Nb and Ta are controlled by the same solution mechanism. A strong 1:1 correlation between Al_2O_3 and Ta_2O_5 in rutile (Fig. 7), for example, verifies that the coupled substitution, $Al^{+3} + Ta^{+5} = 2Ti^{+4}$, is active in experiments doped with Ta_2O_5. This observation is consistent with the coupled substitution, $Al^{+3} + Nb^{+5} = 2Ti^{+4}$, found in experiments doped with only Nb_2O_5 (Fig. 6). The solution mechanism for $TaAlO_4$ is described by homogeneous equilibria

$$AlOAl_{(melt)} + TaOTa_{(melt)} = 2TaOAl_{(melt)} \quad (7)$$

In peraluminous melts in which excess Al exists as tricluster (AlOAl) without SiO_4 tetrahedra (or possibly AlOSi with SiO_4 tetrahedra). The KOTa species in peralkaline melts are similar to those in Nb-bearing peralkaline melts discussed above.

The crystalline phase Ta-Al-rutile in Ta-bearing peraluminous melts is similar to the Nb-Al-rutile in Nb-bearing peraluminous melts. The Ta-Al-rutile is a good analog to naturally occurring Ta-rutile (or struverite) in granite pegmatites except that Fe^{+3} typically replaces Al^{+3} as the charge balancing species for Nb^{+5}. Like ilmenorutile, the struverite $[(Ti, Ta, Fe^{+3})_3O_6]$ has the same structure as rutile, an expected consequence of the similarity of ionic radii of Al^{+3} (0.53 Å) and Fe^{+3} (0.55 Å) in six-fold coordination with oxygen (Foord 1982).

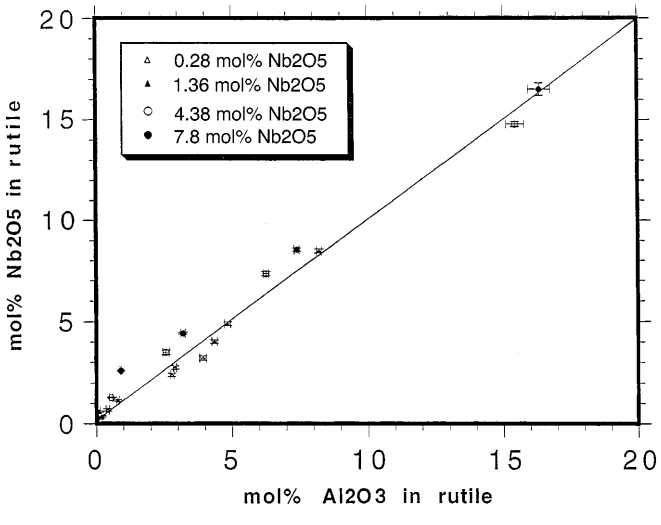

Fig. 6 A coupled substitution, $Al^{+3} + Nb^{+5} = 2Ti^{+4}$, in rutile coexisting with peraluminous melts doped with different amounts of Nb_2O_5 at 1400 °C and 1 atmosphere

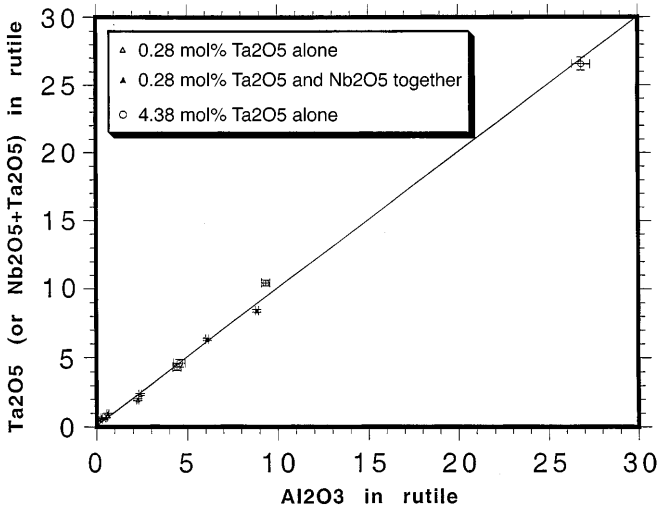

Fig. 7 Coupled substitutions, $Al^{+3} + Ta^{+5} = 2Ti^{+4}$ for 0.28 mol% Ta_2O_5 experiments and $Al^{+3} + (Nb^{+5}, Ta^{+5}) = 2Ti^{+4}$ for 0.28 mol% Nb_2O_5 and Ta_2O_5 together experiments, in rutile coexisting with peraluminous melts at 1400 °C and 1 atmosphere

Melts doped with Nb_2O_5 and Ta_2O_5 together

Partition experiments run with Ta alone or melts doped with Ta + Nb together show that the solution mechanisms for Ta in rutile and melt are similar to those proposed for Nb. A strong 1:1 correlation between Al_2O_3 and Nb_2O_5 + Ta_2O_5 in rutile also verifies the coupled substitution [Al^{+3} + (Ta^{+5}, Nb^{+5}) = $2Ti^{+4}$] in experiments doped with Nb_2O_5 and Ta_2O_5 together (Fig. 8). The D versus K* curves for Ta-doped melts, moreover, parallel those obtained for Nb-doped melts. It follows that the dominant melt species for Ta is $AlTaO_4$ in peraluminous melts and KOTa in peralkaline melts, similar in kind to those in Nb-bearing melts.

Nb_2O_5 and Ta_2O_5 in rutile

The main difference between the Ta- and Nb-bearing systems is that the rutile-melt Ds for Ta are approximately twice as large as those of Nb (Fig. 4). This result is surprising because Nb and Ta possess the same charge (+5) in air at 1 atmosphere, and both possess the same ionic radii (Ta^{+5} = 0.64 Å, Nb^{+5} = 0.64 Å) for six-fold coordination with oxygen (Shannon and Prewitt 1969). The difference between Nb and Ta partitioning into rutile, therefore, is not explained by possible variation in the ionic potential Z/r (where Z = cation charge and r = cation radius) which is one of the most important parameters in estimating cation-oxygen bond strength. One possible explanation for the difference between the partitioning behavior of Nb and Ta is that Nb and Ta exist in different oxidation states under the experimental conditions. Niobium (1.6) is slightly more electronegative than Ta (1.5) according to Pauling's scale (Pauling 1960); therefore, Nb exists in a trivalent state more easily than Ta under the same condition (Green and Pearson 1987). The Nb^{+3} would be less compatible in rutile, since the ionic radius of Nb^{+3} (0.70 Å) is larger than Nb^{+5} (0.64 Å) (Wolff 1984). Under conditions where a substantial amount of Nb exists in its trivalent state, Nb would be excluded more readily from rutile structure than Ta.

It is very unlikely, however, that Nb exists in the two valence states (Nb^{+3} and Nb^{+5}) under the experimental conditions of 1400 °C and melts equilibrated with air. One half of Nb in the melt would have to be in a trivalent state to explain the Ds for Ta and Nb. In addition, if one half of Nb exists in trivalent state in liquid, then some Nb^{+4} would also be stable. The Nb_2O_4 possesses the same structure as rutile (Cotton and Wilkinson 1988), and Nb^{+4} would substitute for Ti^{+4} more readily than either Nb^{+3} or Nb^{+5}. As a result, more than one half of Nb existing in trivalent state is required to compensate for the easy entry of Nb^{+4} into the rutile structure. Furthermore, the oxidation state of Nb depends on temperature, oxygen fugacity, and bulk melt composition. If the different oxidation states of Nb contribute to the difference between the rutile-melt Ds of Nb and Ta, the ratio of the Ds of Ta to Nb would vary at a different K*. The Ds of Ta are approximately twice as large as those of Nb for different bulk melt compositions. This observation suggests that Nb^{+3} is not a predominant factor responsible for the difference in the partitioning behavior of Nb and Ta.

In addition to charge and ionic radius, the polarizability, i.e., the distortion of the electron cloud of an ion caused by an oppositely charged neighbor, is an important factor controlling chemical substitution in crystals.

The polarizing power of Nb and Ta can be evaluated in terms of the specific refractivity of the respective cation. When an atom is subjected to electromagnetic radiation, a temporary displacement of its valence electrons is induced by the electric field of electromagnetic radiation operative at optical frequencies (Jaffe 1988). The induced dipole moment (μ) results from the distortion of the symmetrical electronic charge distribution with respect to the nucleus of the atom. The magnitude of such dipole moments, summed up over all the atoms in a mineral, is determined by the calculation of the molecular electronic polarizability (α_G). The molecular electronic polarizability can be evaluated from measurements of the indices of refraction, density, and molar volume according to the Gladstone-Dale equation (Jaffe 1988):

$$\alpha_G = (3/(4\pi \times N)) \times K_G \times M \quad (8)$$

in which N = Avogadro's number, K_G = the specific refractivity of Nb and Ta in six-fold coordination with oxygen (Jaffe 1988), and M = the molecular weight of the oxide of interest (Nb_2O_5: 265.81; Ta_2O_5: 441.89). The molecular electronic polarizabilities of Nb_2O_5 and Ta_2O_5 calculated from Eq. (8) are 26.239 and 24.274, respectively.

Niobium and Ta exist in NbO_6 and TaO_6 octahedra, and they substitute for octahedrally coordinated Ti in the presence of charge balancing trivalent cation in rutile. The Nb and Ta must compete with Ti for the valence electrons of oxygen, resulting in the weakening of Ti-O bond. The polarizing power of Nb in six-fold coordination is greater than that of Ta in the same coordination. The formation of a strong covalent bond between Nb and O weakens the Ti-O bond more than the interactions between Ta and O, so that the substitution of Nb for Ti distorts the rutile structure more severely than the Ta substitution for Ti. Consequently, a smaller quantity of Nb partitions into rutile than Ta. This enables rutile to maintain same structure, and the structural distortion is minimized.

According to the polarizability argument in which two elements possess identical ionic potential, it is reasonable to conclude that the polarizing power difference between two cations might provide additional insight regarding their partitioning between a crystalline phase and a liquid phase. For example, the partition coefficient of Ta between the crystalline phase and liquid phase in the Ta_2O_5-Nb_2O_5 system is greater than that of Nb

Table 5 Experimental conditions and chemical composition of saturated rutile and coexisting haplogranite melts doped with 1 mol% ZrO_2 and 1 mol% HfO_2 together

Sample	T (°C)	Phase	SiO_2	K_2O	Al_2O_3	TiO_2	ZrO_2	HfO_2	K*	D_{Zr}	D_{Hf}
ZH*001	1400	Melt	76.41 ± 0.63[a]	5.77 ± 0.14	10.39 ± 0.27	6.68 ± 0.21	0.35 ± 0.08	0.40 ± 0.06	0.36	43.90	72.12
		Rutile	0.03 ± 0.02	0.07 ± 0.03	0.70 ± 0.03	55.50 ± 0.39	15.23 ± 0.23	28.49 ± 0.29			

[a] The values before the ± symbol refer to analytic results (mol%), and the values after the ± symbol denote one standard error (wt%)

(Holtzberg and Reisman 1961), since the polarizing power of Ta^{+5} is less than that of Nb^{+5}. In another example, the ionic potentials of Zr (Z/r = +4/0.71 Å for six-fold coordination) and Hf (Z/r = +4/0.72 Å for the same coordination) are very close. However, the D of Hf between rutile and melt is about 1.6 times as much as that of Zr in rutile saturation experiments with the same system, K* = 0.35, doped with 1 mol% Zr_2O_5 and 1 mol% Hf_2O_5 at 1400 °C and 1 atmosphere (Table 5). This result is consistent with the observation that the molecular electronic polarizabilities of ZrO_2 and HfO_2 are 10.35 and 9.64 $(Å)^3$ respectively (Table 6).

Concluding remarks

Partition coefficients of Nb and Ta between rutile and haplogranite melts are strong functions of bulk composition as measured by K*, the concentration of Nb_2O_5 and Ta_2O_5 and temperature. The partition coefficients are rationalized by proposing that the activity of $NbAlO_4$ species in peraluminous melts and the activity of KONb species in peralkaline melts control the rutile-melt equilibria. The extraordinarily large Nb (Ta) rutile-melt partition coefficients in peraluminous melts are a consequence of the coupled substitution of $Al^{+3} + Nb^{+5} = 2Ti^{+4}$ which allows easy entry of Nb (Ta) into the rutile structure. The high activity of $NbAlO_4$ in peraluminous melts and the low activity of this species in peralkaline melts account for the large differences in the partition coefficients between peraluminous and peralkaline melts.

The Ds of Ta between rutile and melts are approximately twice as large as those of Nb in experiments doped with Nb_2O_5 and Ta_2O_5 together. This difference cannot be explained by their ionic potentials, but rather by the contrasting polarizabilities. The Nb^{+5} with a large polarizing power forms a stronger covalent bond with oxygen than Ta^{+5} with a smaller polarizing power.

Table 6 Ionic potential Z/r (where Z = cation charge and r = ionic radii in Å) and molecular electronic polarizability α_G in $(Å)^3$ of Nb, Ta, Zr, and Hf

Cation	Ionic potential (Z/r)	Molecular electronic polarizability α_G
Nb	5/0.64	26.24
Ta	5/0.64	24.27
Zr	4/0.71	10.34
Hf	4/0.72	9.64

The formation of the strong bond, Nb-O, distorts the rutile structure more severely than the weak bond, Ta-O. Therefore, it is more favorable for Ta to partition into rutile than for Nb.

Niobium and Ta normally are considered as geochemical twins due to their same charges and ionic radii. The ratio of Nb to Ta is, therefore, expected to be constant within a co-magmatic suite, thus allowing the Nb/Ta ratio to be used as a petrogenetic indicator of distinct source regions with different Nb/Ta ratios. The partition coefficients of Ta between rutile and melts, however, are approximately twice as large as those of Nb. The utilization of the Nb/Ta ratio as a petrogenetic indicator in granitic melts must be done with caution if rutile (or other TiO_2-rich phases) is a liquidus phase because the Nb/Ta ratio of the residual liquid increases with rutile crystallization. The petrogenetic consequences of such equilibria are discussed more fully in a companion paper (W.-S. Horng and P.C. Hess in preparation).

Acknowledgements We are grateful to Stu McCallum and an anonymous reviewer for useful criticism. This work was supported by NSF grant EAR-9304046.

References

Abella PA, Cordomi MC, Draper JC (1995) Nb-Ta minerals from the Cap de Creus pegmatite field, eastern Pyrenees: distribution and geochemical trends. Mineral Petrol 55: 53–69

Cerny P (1992) Rare-element granitic pegmatites. 1. Anatomy and internal evolution of pegmatite deposits. Geosci Can 18: 68–81

Cerny P, Chapman R, Simmons WB, Chackowsky LE (1999) Nioban rutile from the McGuire granitic pegmatite Park County, Colorado: solid solution, exsolution and oxidation. Am Mineral 84: 754–763

Cotton FA, Wilkinson G (1988) Advanced inorganic chemistry. John Wiley and Sons, New York, pp 776–804

Dickinson JE, Hess PC (1985) Rutile solubility and Ti coordination in silicate melts. Geochim Cosmoschim Acta 49: 2289–2296

Foord EE (1982) Minerals of tin, titanium, niobium, and tantalum in granitic pegmatites. In: Cerny P (ed) Granitic pegmatites in science and industry. Mineral Assoc Can Short-Course Handb 8, pp 187–238

Gan H, Hess PC (1992) Phosphate speciation in potassium aluminosilicate glasses. Am Mineral 77: 495–506

Gan H, Hess P, Horng WS (1994) P^{5+}, Nb^{5+} and Ta^{5+} interactions with anhydrous haplogranite melts. EOS Trans Am Geophys Union 75: 369

Green TH, Pearson NJ (1987) An experimental study of Nb and Ta partitioning between Ti-rich minerals and silicate liquids at high pressure and temperature. Geochim Cosmochim Acta 51: 55–62

Hess PC (1991) The role of high field strength cations in silicate melts. In: Perchuk LL, Kushiro I (eds) Physical chemistry of magmas. (Advances in Geochemistry, vol 9) Springer Verlag, Berlin Heidelberg New York Tokyo, pp 152–191

Hess PC (1995) Thermodynamic mixing properties and the structure of silicate melts. In: Stebbins JF, McMillan PF, Dingwell DB (eds) Structure, dynamics and properties of silicate melts. (Reviews in mineralogy, vol. 32) Mineral Assoc Am Short-Course Handb, pp 145–189

Holtzberg F, Reisman A (1961) Sub-solidus equilibria in the system Nb_2O_5-Ta_2O_5. J Phys Chem 65: 1192–1196

Horng W, Hess CP, Gan H (1999) The interaction between M^{+5} cations (Nb^{+5}, Ta^{+5} or P^{+5}) and anhydrous haplogranite melts. Geochim Cosmochim Acta 63: 2419–2428

Jaffe HW (1988) Crystal chemistry and refractivity. Cambridge, University Press, Cambridge, p118–140

Lacey ED (1968) Configuration change in silicates with particular reference to network structures. Acta Crystallogr 18: 141–150

London D (1992) The application of experimental petrology to the genesis and crystallization of granitic pegmatites. Can Mineral 30: 449–540

McCallum IS, Charette MP (1978) Zr and Nb partition coefficients: implications for the genesis of Mare basalts, Kreep, and sea floor basalts. Geochim Cosmochim Acta 42: 859–869

McMillan P, Piriou B (1982) The structures and vibrational spectra of crystals and glasses in the silica-alumina system. J Non-Cryst Solids 53: 279–298

McMillan P, Piriou B, Navrotsky A (1982) A Raman spectroscopic study of glasses along the joins silica-calcium aluminate, silica-sodium aluminate, and silica-potassium aluminate. Geochim Cosmochim Acta 46: 2021–2037

Mysen BO, Virgo D, Scarf CM (1980) Relations between the anionic structure and viscosity of silicate melts, a Raman spectroscopic study. Am Mineral 65: 690–710

Mysen BO, Virgo D, Kushiro I (1981) The structural role of aluminum in silicate melts – a Raman spectroscopic study at 1 atmosphere. Am Mineral 66: 678–701

Mysen BO, Virgo D, Seifert FA (1982) The structure of silicate melts: implication for chemical and physical properties of natural magma. Rev Geophys 20: 353–383

Pauling L (1960) The nature of the chemical bond, 3rd edn. Cornell Univ Press, New York

Sato RK, McMillan PF, Dennison P, Dupree R (1991) A structural investigation of high alumina glasses in the CaO-Al_2O_3-SiO_2 system via Raman and magic angle spinning nuclear magnetic resonance spectroscopy. Phys Chem Glasses 33: 149–156

Shannon RD, Prewitt CT (1969) Effective ionic radii in oxides and fluorides. Acta Crystallogr 25: 925–946

Sharma SK, Virgo D, Mysen BO (1978) Structure of glasses and melts of $Na_2O{\cdot}xSiO_2$ (x = 1, 2, 3) composition from Raman spectroscopy. Carnegie Ins Washington Yearb 77: 649–652

Virgo D, Seifert F, Mysen BO (1979) Three dimensional network structures of glasses in the systems $CaAl_2O_4$-SiO_2, $NaAlO_2$-SiO_2, $NaFeO_2$-SiO_2 and $NaGaO_2$-SiO_2 at 1 atmosphere. Carnegie Inst Washington Yearb 78: 506–511

Wolff JA (1984) Variation in Nb/Ta during differentiation of phonlitic magma, Tenerife, Canary Islands. Geochim Cosmochim Acta 48: 1345–1348